Suppressing nonadiabatic transitions during adiabatic generation of highly entangled states in bosonic Josephson junctions

Takuya Hatomura*
NTT Basic Research Laboratories, NTT Corporation, Kanagawa 243-0198, Japan

(Received 16 July 2019; published 31 October 2019)

We study suppression of nonadiabatic transitions during adiabatic generation of a catlike state (a superposition of different-sized cat states) and a spin squeezed state in a bosonic Josephson junction. In order to minimize the adiabatic error, we use the quantum adiabatic brachistochrone, which enables us to track a geometrically efficient path in parameter space under given conditions without requiring additional terms. For the creation of a catlike state, divergence of the quantum geometric tensor associated with gap closing at the critical point is avoided because of the parity conservation. The resulting schedules of parameters are smooth and monotonically decreasing curves. Use of these schedules offers a reduction in the time to generate both a catlike state and a spin squeezed state.

DOI: 10.1103/PhysRevA.100.043619

I. INTRODUCTION

Development of quantum science and technologies has elucidated the usefulness of entanglement. In many fields, use of entangled states enables us to outperform classical devices [1]. For example, in quantum metrology, we can produce sensors that estimate unknown parameters with higher resolution than the classical limitation called the standard quantum limit [2–4]. Moreover, macroscopic entanglement provides us with significant resolution approaching the quantum limitation known as the Heisenberg limit [2–4]. Unknown parameters that we can estimate differ depending on the physical systems, and thus generation of highly entangled states has been investigated in various systems. In atomic systems, a lot of successful experiments generating spin squeezed states have been reported [5–13]. The number of particles composing these spin squeezed states is suitable to be called macroscopic (see, e.g., Ref. [4]). Moreover, cat states have also been produced in trapped ions [14–16]. However, in contrast to spin squeezed states, the number of particles composing cat states is still limited to a dozen.

Typically, these highly entangled states can be dynamically generated by using a one-axis twisting interaction [17]. Indeed, the one-axis twisting interaction transforms a coherent spin state into a spin squeezed state at first [17] and into a cat state later [18]. However, the generation time of a cat state is not very short, and thus it is difficult to create a large cat state within the coherence time. Faster generation can be realized by just adding Rabi coupling to the one-axis twisting interaction [19], while fidelity to a cat state decreases when the system size becomes large. Since these generation schemes were proposed, some tricks to improve dynamical generation have been discussed [20,21]. Not only do the generation time and size of entanglement present difficulties, but also the termination of creation at the final time. Because these generation schemes are based on dynamical interference driven by nonlinear interactions, we have to turn off all interactions at the final time. Otherwise, highly entangled states collapse into useless states.

These highly entangled states can be also generated by adiabatic driving. Indeed, with certain parameter values, the ground state of a system consisting of a one-axis twisting interaction and Rabi coupling is a spin squeezed state for repulsive interaction [22] and that is a cat state for attractive interaction [23]. Note that it is difficult to directly approach these ground states by cooling down alone because of small energy gaps. In adiabatic generation, we first prepare the trivial ground state in the large Rabi coupling limit, and we then adiabatically sweep parameters into the large one-axis twisting interaction limit [23–27]. Notably the generation time of a cat state is comparable to the typical coherence time [27]. However, the size of generated cat states can still reach only up to $N = 20$ [16]. This limitation mainly arises from particle losses [28,29]. Particle losses induce various noises during generation and destroy entanglement. Because particle losses are inevitable in ultracold-atom experiments, speedup of generation is rather of interest to reduce this bad influence.

In both dynamical and adiabatic generation of spin squeezed states, application of optimal control theory and shortcuts to adiabaticity have been discussed and speedup of generation was found [30–34]. However, optimal control theory usually requires fast and irregular oscillating schedules of parameters [30,33], which induce nonadiabatic transitions and interference to finally achieve high fidelity to a target state, and thus experimental implementation is not very straightforward. Shortcuts to adiabaticity also require oscillating schedules of parameters, whereas oscillation of these schedules is relatively slow [31,32,34]. For creation of cat states, application of optimal control theory and shortcuts to adiabaticity was also considered [35,36]. In the former case, fast and irregular oscillating schedules and turning-off of all interactions at

*takuya.hatomura.ub@hco.ntt.co.jp

last are required to accelerate dynamical generation [35]. In the latter case, a two-axis countertwisting interaction [17] is additionally required to speed up adiabatic generation [36]. However, in spite of the fact that the usefulness of the two-axis countertwisting interaction for fast generation of macroscopic entanglement was pointed out about a quarter-century ago [17] and many methods for realization have been proposed [37–41], there has been no experimental realization of it in atomic systems yet. Therefore, other realistic routes to fast generation should be investigated. It is also noteworthy that in the context of shortcuts to adiabaticity generation of this type of cat state was first discussed in the transverse Ising model, where not only two-axis countertwistinglike interaction but also much higher-order interactions are required [42].

The quantum adiabatic brachistochrone is a systematic method to find a time-optimal schedule of parameters in a system [43,44]. A cost function of the adiabatic condition is viewed as the action and minimized according to the variational principle. The resulting Euler-Lagrange equation gives the geodesic equation for adiabaticity and provides a schedule of parameters. Compared with counterdiabatic driving [45,46], which is one method of shortcuts to adiabaticity [47], the quantum adiabatic brachistochrone does not require additional terms, and thus it is rather implementable.

In this paper, we use the quantum adiabatic brachistochrone to suppress nonadiabatic transitions during adiabatic generation of a catlike state and a spin squeezed state at a bosonic Josephson junction without requiring additional terms. We show that optimized schedules for adiabatic generation of both a catlike state and a spin squeezed state are smooth and monotonically decreasing curves. Here, for creation of a catlike state, we use the parity conservation of a bosonic Josephson junction to avoid divergence of the quantum geometric tensor. According to these schedules, we observe an increase in quantum Fisher information for a generated catlike state and a decrease in the spin squeezing parameter for a generated spin squeezed state, which represent an improvement of adiabaticity and an increase in metrological usefulness.

This paper is constructed as follows. In Sec. II, we review the properties of bosonic Josephson junctions and formalism of the quantum adiabatic brachistochrone. Generation schemes are explained in Sec. III A in detail. We first discuss the generation of catlike states in Sec. III B and then discuss the generation of spin squeezed states in Sec. III C. We summarize the present article in Sec. IV.

II. METHODS

A. Bosonic Josephson junctions

Bosonic Josephson junctions consist of two species of bosons, a_1 and a_2, which are realized in various systems including the low-energy limit of Bose-Einstein condensates [48]. The Hamiltonian of a bosonic Josephson junction is given by

$$\mathcal{H}_{\mathrm{BJJ}} = \hbar\chi J_z^2 + \hbar\Omega J_x, \tag{1}$$

where χ is the Kerr nonlinearity, Ω is the Rabi coupling, and J_α, $\alpha = x, y, z$ is the angular momentum representation of bosonic operators:

$$\begin{cases} J_x = \dfrac{1}{2}(a_1^\dagger a_2 + a_2^\dagger a_1), \\ J_y = \dfrac{1}{2i}(a_1^\dagger a_2 - a_2^\dagger a_1), \\ J_z = \dfrac{1}{2}(a_1^\dagger a_1 - a_2^\dagger a_2). \end{cases} \tag{2}$$

The first term is also known as the one-axis twisting interaction [17]. This system is characterized by the parameter

$$\Lambda = \frac{\chi N}{\Omega}, \tag{3}$$

where N is the number of atoms. Here we assume $\Omega \leqslant 0$.

For positive nonlinearity $\chi > 0$, the ground state of Hamiltonian (1) becomes a spin squeezed state, where fluctuation along the z axis, ΔJ_z, is suppressed and fluctuation along the y axis, ΔJ_y, is enhanced, when the parameter Λ^{-1} is small, $|\Lambda^{-1}| < 1$ [22]. This type of spin squeezed states has been realized in experiments by adiabatically splitting condensates [5]. The level of squeezing depends on the competition between adiabaticity and losses, i.e., how slowly parameters change to suppress nonadiabatic transitions and how quickly a spin squeezed state is generated to suppress the bad influence of particle losses [8]. Therefore, speedup of generation is of interest.

In contrast, for negative nonlinearity $\chi < 0$, a cat state, a superposition of a mode 1 condensate and a mode 2 condensate, can be realized as the ground state of Hamiltonian (1) for $0 \leqslant \Lambda^{-1} < 1$ [23]. However, creation of this cat state would fail if one just cooled the system in this parameter region due to the occurrence of spontaneous symmetry breaking. This happens because of the exponentially small energy gap between the ground state and the first excited state. Adiabatic generation is one of the strategies for creating this cat state [23,26,27]. The key point of adiabatic generation is parity conservation [27], ensured by the commutation relation

$$[\mathcal{H}_{\mathrm{BJJ}}, \Pi] = 0, \tag{4}$$

where Π is the parity operator

$$\Pi = \exp[i\pi(J - J_x)]. \tag{5}$$

In adiabatic generation, we start with the trivial ground state of Hamiltonian (1) in the disordered phase $\Lambda^{-1} > 1$, which has the parity $\Pi = +1$. Because the first excited state has parity $\Pi = -1$ and the parity is conserved in time evolution, we can ignore the exponentially small energy gap [27]. The parity conservation also ensures that the generated state is rather a superposition of different-sized cat states [49],

$$\begin{aligned} |\Psi\rangle &= \sum_m g_m |\Psi_m\rangle, \\ |\Psi_m\rangle &= \frac{1}{\sqrt{2}}(|N-m, m\rangle + |m, N-m\rangle), \end{aligned} \tag{6}$$

where $\sum_m |g_m|^2 = 1$. Therefore, the generated state is close to a cat state (the NOON state) if $\{|g_m|^2\}$ is distributed around $m \approx 0$. It was shown that parity measurement and Fourier analysis enable us to detect this superposition including the information on the size distribution of these cat states $\{|g_m|^2\}$

and also to maximally extract the potential of this superposition in interferometry [49]. However, these properties are lost in an exponential way under particle losses, although its decay rate is lower than that of dynamical generation [49], and thus we are interested in acceleration of generation.

B. Quantum adiabatic brachistochrone

The quantum adiabatic brachistochrone provides us with systematic temporal optimization of Hamiltonians to achieve adiabatic time evolution [43,44]. Here we briefly review this method.

For a given Hamiltonian $\mathcal{H}(\boldsymbol{\lambda};s)$, the dynamical transformation is a unitary operator $V(s)$ that defines the time evolution of a given state

$$|\Psi(s)\rangle = V(s)|\Psi(0)\rangle \tag{7}$$

by the Schrödinger dynamics

$$i\hbar\frac{\partial}{\partial s}V(s) = T\mathcal{H}(\boldsymbol{\lambda};s)V(s), \tag{8}$$

where $s = t/T$ is the normalized time and T is the operation time. Here we assume that the Hamiltonian depends on time through time-dependent parameters $\boldsymbol{\lambda}(s) = (\lambda_1, \lambda_2, \ldots, s)$. For the same Hamiltonian, the adiabatic transformation is a unitary operator $V_{\rm ad}(s)$ that isometrically transforms the projection operators as

$$V_{\rm ad}(s)P_n(\boldsymbol{\lambda};0)V_{\rm ad}^\dagger(s) = P_n(\boldsymbol{\lambda};s) \tag{9}$$

for all n, where

$$\mathcal{H}(\boldsymbol{\lambda};s)P_n(\boldsymbol{\lambda};s) = E_n(\boldsymbol{\lambda};s)P_n(\boldsymbol{\lambda};s), \tag{10}$$

with the eigenenergy $E_n(\boldsymbol{\lambda};s)$. The adiabatic transformation generates adiabatic time evolution

$$|\Psi_{\rm ad}(s)\rangle = V_{\rm ad}(s)|\Psi(0)\rangle. \tag{11}$$

There exists a Hamiltonian $\mathcal{H}_{\rm ad}(s)$ that generates adiabatic time evolution, (11), as the Schrödinger dynamics

$$i\hbar\frac{\partial}{\partial s}V_{\rm ad}(s) = T\mathcal{H}_{\rm ad}(s)V_{\rm ad}(s). \tag{12}$$

This adiabatic Hamiltonian $\mathcal{H}_{\rm ad}(s)$ is given by

$$\mathcal{H}_{\rm ad}(s) = \mathcal{H}(\boldsymbol{\lambda};s) + \frac{i\hbar}{T}[\partial_s P_n(\boldsymbol{\lambda};s), P_n(\boldsymbol{\lambda};s)] \tag{13}$$

for a given state in the nth eigensector of the Hamiltonian $\mathcal{H}(\boldsymbol{\lambda};s)$ [50]. Note that, in the context of shortcuts to adiabaticity [47], the additional term is nothing but the single-spectrum counterdiabatic term [51]. If we consider the adiabatic transformation of the full eigensectors of the Hamiltonian, we should introduce the usual counterdiabatic terms [45,46] instead of Eq. (13).

Deviation of the dynamical transformation from the adiabatic transformation can be estimated by using the wave operator

$$\Omega(s) = V_{\rm ad}^\dagger(s)V(s), \tag{14}$$

satisfying the Volterra equation

$$\Omega(s) = 1 - \int_0^s K_T(s')\Omega(s')ds', \tag{15}$$

with the kernel

$$K_T(s) = V_{\rm ad}^\dagger(s)[\partial_s P(\boldsymbol{\lambda};s), P(\boldsymbol{\lambda};s)]V_{\rm ad}(s), \tag{16}$$

where $\Omega(s)$ is close to 1 when the dynamical transformation is close to adiabatic transformation. Our goal is to minimize $1-\Omega(s)$ and it is achieved by minimizing the action

$$\epsilon[\boldsymbol{\lambda}(s)] = \int_0^s \|[\partial_{s'}P_n(\boldsymbol{\lambda};s'), P_n(\boldsymbol{\lambda};s')]\|ds', \tag{17}$$

where the norm $\|\cdot\|$ is the operator norm. We can rewrite this action as

$$\epsilon[\boldsymbol{\lambda}(s)] = \int_0^s \sqrt{2g_{ij}\dot{\lambda}^i\dot{\lambda}^j}ds', \tag{18}$$

with the metric

$$g_{ij} = \mathrm{Re}\left[\sum_{m\neq n}\frac{\langle\Psi_n|\partial_i\mathcal{H}|\Psi_m\rangle\langle\Psi_m|\partial_j\mathcal{H}|\Psi_n\rangle}{(E_m-E_n)^2}\right], \tag{19}$$

which is known as the quantum geometric tensor. The Euler-Lagrange equation leads to the geodesic equation

$$\ddot{\lambda}^i + \Gamma^i_{jk}\dot{\lambda}^j\dot{\lambda}^k = 0, \tag{20}$$

with

$$\Gamma^i_{jk} = \tfrac{1}{2}g^{il}(\partial_k g_{li} + \partial_j g_{lk} - \partial_l g_{jk}). \tag{21}$$

This geodesic equation gives an optimal schedule of parameters under a given initial condition (for the detailed derivation, see Ref. [44]).

III. RESULTS

A. Setups

We rewrite the bosonic Josephson junction Hamiltonian, (1), as

$$\mathcal{H}_{\rm BJJ} = \mathrm{sgn}(\chi)\left(\frac{1}{N}J_z^2 + \Lambda^{-1}J_x\right) \tag{22}$$

and set the rescaled time $\tau = |\chi|Nt$ with fixed χ. Then the time dependence of the Hamiltonian comes only from Λ^{-1}. Note that this rescaled time differs from the normalized time in the previous section. We simulate the rescaled Schrödinger equation

$$i\frac{\partial}{\partial\tau}|\Psi(\tau)\rangle = \mathcal{H}_{\rm BJJ}|\Psi(\tau)\rangle. \tag{23}$$

As the initial state, we prepare the coherent spin state along the x axis,

$$|\Psi(0)\rangle = 2^{-N/2}\sum_{n=0}^{N}\sqrt{\binom{N}{n}}|J, J-n\rangle. \tag{24}$$

The parity of this state is $\Pi = +1$ and it is close to the ground state of the Hamiltonian with $|\Lambda^{-1}| > 1$.

We determine the time dependence of the parameter Λ^{-1} according to the geodesic equation, (20), for adiabaticity. For a single parameter, $\lambda = \Lambda^{-1}$, the geodesic equation, (20), reduces to [44]

$$2g\ddot{\lambda} + (\partial_\lambda g)\dot{\lambda}^2 = 0. \tag{25}$$

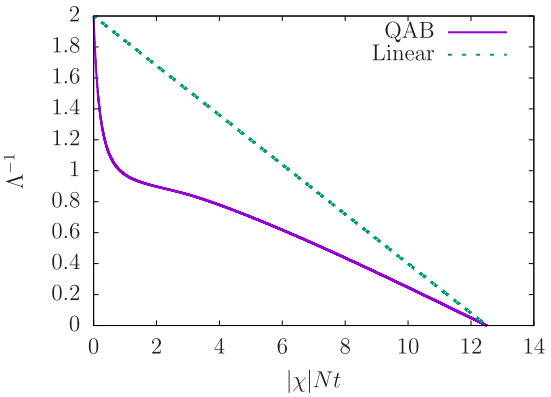

FIG. 1. An example of schedules of Λ^{-1} with respect to the rescaled time $|\chi|Nt$. The solid purple curve represents the schedule based on the quantum adiabatic brachistochrone for $C = -0.5$ and the dotted green line represents the linear schedule with the same generation time. Here $N = 100$.

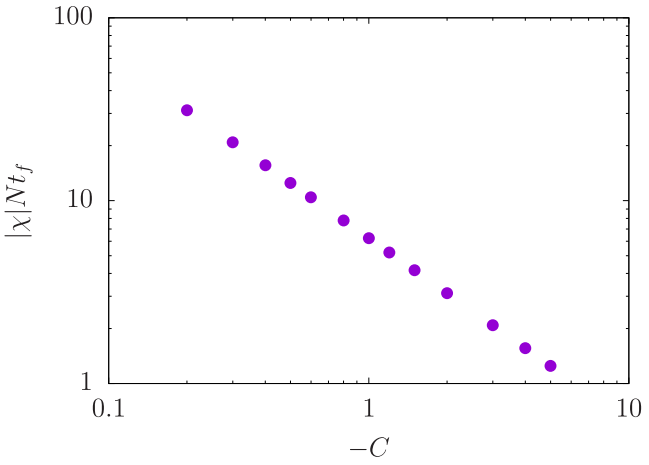

FIG. 2. The constant C dependence of the rescaled generation time $|\chi|Nt_f$. Here $N = 100$.

We can numerically solve this equation by giving the initial parameter $\lambda(0)$ and the time derivative of the initial parameter $\dot{\lambda}(0)$. The equality

$$\frac{d}{d\tau}(\sqrt{g}\dot{\lambda}) = \frac{1}{2\sqrt{g}}[2g\ddot{\lambda} + (\partial_\lambda g)\dot{\lambda}^2] = 0 \tag{26}$$

holds, and thus we can also rewrite the geodesic equation, (25), as

$$\sqrt{g}\dot{\lambda} = C, \tag{27}$$

with a constant C. In this case, we can numerically solve this equation by giving the initial parameter $\lambda(0)$ and giving a certain constant C instead of $\dot{\lambda}(0)$. Note that the metric g is simply given by

$$g = \sum_{m\neq n} \frac{|\langle\Psi_m|(\partial_\lambda \mathcal{H}_{\rm BJJ})|\Psi_n\rangle|^2}{(E_m - E_n)^2}. \tag{28}$$

Because the parameter derivative of the Hamiltonian $(\partial_\lambda \mathcal{H}_{\rm BJJ})$ and the parity operator Π are commutative, i.e.,

$$[(\partial_\lambda \mathcal{H}_{\rm BJJ}), \Pi] = 0, \tag{29}$$

we can reduce summation in the metric, (28), so that the eigenstate $|\Psi_m\rangle$ has a parity identical to that of $|\Psi_n\rangle$. This reduction is quite important for the present generation schemes because we can avoid numerical divergence associated with gap closing and with the degeneracies of the eigenstates.

B. Generation of cat states

First, we consider negative nonlinearity $\chi < 0$ to create a catlike state. We change the parameter Λ^{-1} from 2 to 0. An example of schedules optimized by the quantum adiabatic brachistochrone is shown in Fig. 1 with the corresponding linear schedule, $\lambda(\tau) = (\tau/\tau_f)\lambda(\tau_f) + (1 - \tau/\tau_f)\lambda(0)$, where $\tau_f = |\chi|Nt_f$ is the generation time. Here we set $\lambda(0) = 2$, $\lambda(\tau_f) = 0$, and $C = -0.5$. The quantum adiabatic brachistochrone suggests a rapid decrease before approaching the critical point, $\Lambda^{-1} \gtrsim \Lambda_c^{-1} = 1$ (in the disordered phase), and a decrease after passing this (above the critical point and in the ordered phase). We can observe similar schedules with different generation times t_f when we set other values of the constant C. The relationship between the generation time t_f and the constant C is shown in Fig. 2. It clearly indicates $t_f \propto C^{-1}$. Indeed, from Eq. (27), we can obtain

$$\tau = C^{-1}\int_{\lambda(0)}^{\lambda(\tau)} \sqrt{g}d\lambda. \tag{30}$$

Because g is a function of λ, the generation time t_f is inversely proportional to the constant C.

Now we study the generation of a catlike state according to the schedules obtained by the quantum adiabatic brachistochrone (Fig. 1). Here we calculate the quantum Fisher information F_Q, which is a measure of the macroscopicity of entanglement and related to the uncertainty of estimation as $\Delta\theta = 1/\sqrt{F_Q}$ for an unknown parameter θ, with various values of the constant C. We set the interferometric axis to J_z, i.e., the quantum Fisher information is given by

$$F_Q[|\Psi(\tau_f)\rangle, J_z] = 4(\Delta J_z)^2, \tag{31}$$

where $(\Delta J_z)^2$ is the variance of J_z with the state $|\Psi(\tau_f)\rangle$. Here, from Eq. (31), the maximum value of the quantum Fisher information with J_z is N^2. It is known that with a local operator, such as J_z, a given state is at least entangled if the quantum Fisher information is larger than N and a given state is macroscopically entangled if the quantum Fisher information scales as N^2 (see, e.g., Ref. [4]). In the present generation scheme, the large amount of quantum Fisher information ensures a low excess energy, i.e., the generated state is close to a cat state, and potential usefulness in interferometry using the parity measurement [49]. Here we plot the rescaled quantum Fisher information F_Q/N^2 with respect to the rescaled generation time $|\chi|Nt_f$ in Fig. 3, where filled symbols represent the results by the quantum adiabatic brachistochrone and the open symbols represent the results by the linear schedule. Clearly the quantum adiabatic brachistochrone improves the adiabaticity. Note that quantum Fisher information monotonically increases during generation with the quantum adiabatic brachstochrone as shown in Fig. 4,

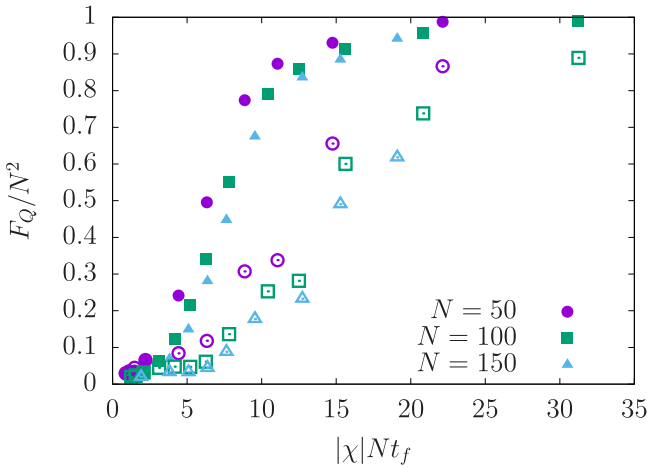

FIG. 3. The rescaled quantum Fisher information F_Q/N^2 with respect to the rescaled generation time $|\chi|Nt_f$. Filled symbols represent the quantum adiabatic brachistochrone and open symbols represent the linear schedule. Here $N = 50$ (purple circles), 100 (green squares), and 150 (cyan triangles).

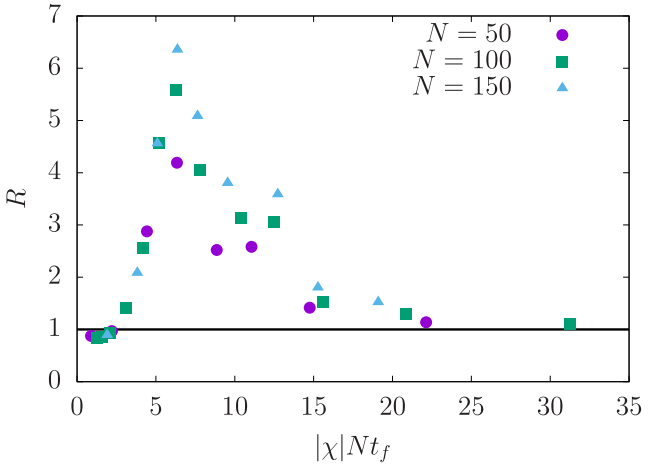

FIG. 5. The rate of improvement in quantum Fisher information $R = F_Q^{\mathrm{QAB}}/F_Q^{\mathrm{Linear}}$ with respect to the rescaled generation time $\tau_f = |\chi|Nt_f$. Here $N = 50$ (purple circles), 100 (green squares), and 150 (cyan triangles). We also plot the supplemental black line, $R = F_Q^{\mathrm{QAB}}/F_Q^{\mathrm{Linear}} = 1$.

where the rescaled quantum Fisher information F_Q/N^2 is plotted with respect to the rescaled time $|\chi|Nt$.

It is of interest whether or not the present results can scale with the system size. In Fig. 3, we find that the rescaled quantum Fisher information F_Q/N^2 versus the rescaled generation time $|\chi|Nt_f$ does not make a big difference except for small finite-size corrections when we change the system size N from 50 to 150. Here we further study how much the quantum adiabatic brachistochrone improves the quantum Fisher information compared with that of the linear schedule. We plot the improving rate $R = F_Q^{\mathrm{QAB}}/F_Q^{\mathrm{Linear}}$ in Fig. 5, where F_Q^{QAB} (F_Q^{Linear}) is the quantum Fisher information of the generated state by the quantum adiabatic brachistochrone (the linear schedule). The improving rate R also shows a similar behavior when we change the system size N. The important point is that the quantum adiabatic brachistochrone improves the quantum Fisher information by more than double in the fast-generation-time regime $4 \lesssim |\chi|Nt_f \lesssim 14$, where a large amount of quantum Fisher information can be obtained by the quantum adiabatic brachistochrone. It is also important that the rate of improvement becomes large when we increase the system size N.

We now discuss why the schedules obtained by the quantum adiabatic brachistochrone take the form of Fig. 1 and why they can improve the adiabaticity. We plot a part of the energy spectrum in Fig. 6. Clearly it shows small energy gaps around the critical point $\Lambda_c^{-1} = 1$ (although there are some finite-size corrections), and thus we have to slowly change the parameter around there. We can see an increase in the energy differences when the parameter becomes small, but the quantum adiabatic brachistochrone still suggests changing the parameter slowly. We can confirm this reason by calculating

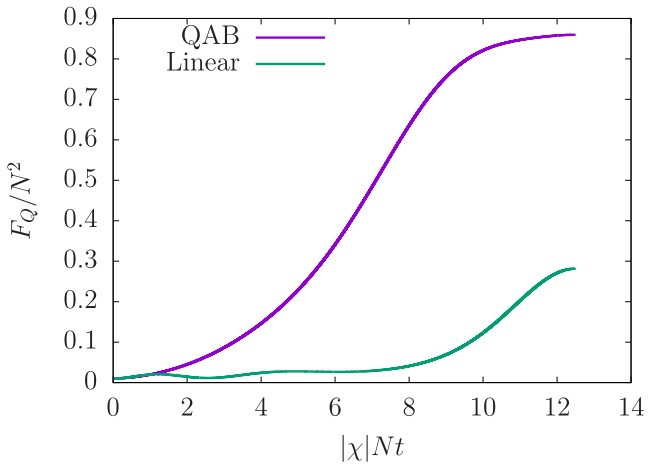

FIG. 4. Growth of quantum Fisher information with respect to the rescaled time $|\chi|Nt$. The purple curve represents the quantum adiabatic brachistochrone and the green curve represents the linear schedule. Here $C = -0.5$ and $N = 100$.

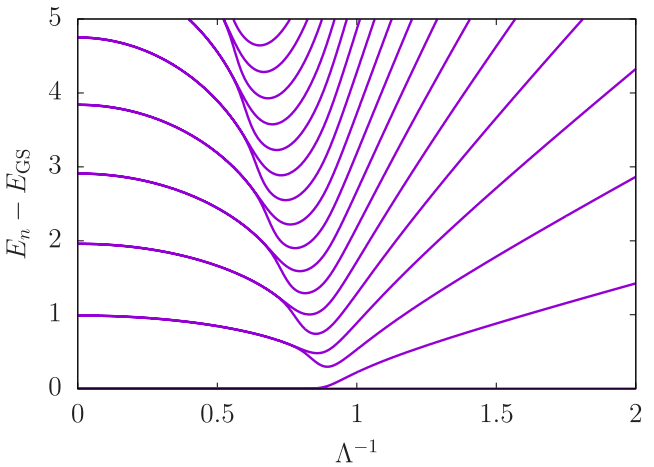

FIG. 6. The energy spectrum $\{E_n - E_0\}$ with respect to the parameter Λ^{-1}. Here $N = 100$.

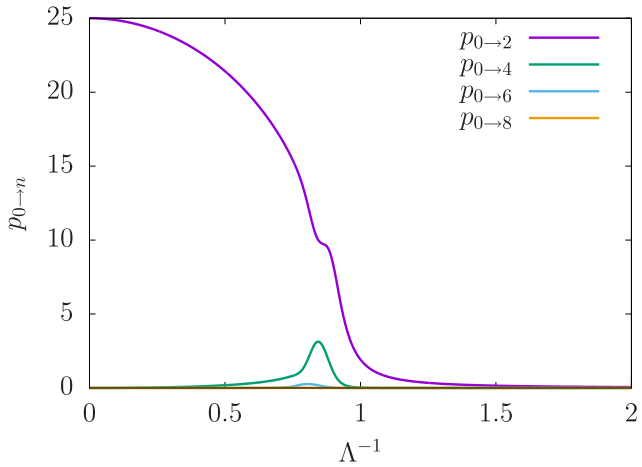

FIG. 7. A part of the transition matrices from the ground state to excited states as functions of Λ^{-1}. Here $N = 100$.

the transition matrices

$$p_{0\to n} = |\langle \Psi_n(\tau)|(\partial_\lambda \mathcal{H}_{\rm BJJ})|\Psi_0(\tau)\rangle|^2. \tag{32}$$

Here we plot some of the main contributions in Fig. 7. We find that the transition matrix from the ground state to the second excited state $p_{0\to 2}$ becomes large when the parameter Λ^{-1} decreases, in contrast to a decrease in other elements. This is why the quantum adiabatic brachistochrone suggests a slow decrease even though the energy differences become large. Note that the transition matrices from the ground state to odd-numbered excited states vanish due to the parity conservation.

C. Generation of spin squeezed states

Next, we consider positive nonlinearity $\chi > 0$ to create a spin squeezed state. An example of schedules optimized by the quantum adiabatic brachistochrone is shown in Fig. 8. In contrast to the case of negative nonlinearity $\chi < 0$, the quantum adiabatic brachistochrone just suggests a fast decrease at first and an extremely slow decrease around $|\Lambda^{-1}| \approx 0$. However, this final slow process does not contribute very much to spin squeezing. In order to show it, we consider two cases, $|\Lambda^{-1}| : 2 \to 0$ and $|\Lambda^{-1}| : 2 \to 0.005$, with $C = -0.07$. The operation time of the case $|\Lambda^{-1}| : 2 \to 0$ is about $\chi N t_f = 29.0$, while that of the case $|\Lambda^{-1}| : 2 \to 0.005$ is about $\chi N t_f = 12.5$. To decrease the parameter $|\Lambda^{-1}|$ from 0.005 to 0, we need an additional generation time $\chi N t = 16.5$, which is longer than the time to decrease $|\Lambda^{-1}|$ from 2 to 0.005. Nevertheless, the spin squeezing parameter

$$\xi_S^2 = \frac{N(\Delta J_z)^2}{\langle J_x\rangle^2}, \tag{33}$$

which is related to the uncertainty of estimation as $\Delta\theta = \xi_S/\sqrt{N}$ for an unknown parameter θ and thus a given state is metrologically useful if $\xi_S < 1$, does not change very much during the process $|\Lambda^{-1}| : 0.005 \to 0$ as shown in Fig. 9. Therefore, hereafter we only consider the process $|\Lambda^{-1}| : 2 \to 0.005$. Note that in contrast to the case of the quantum Fisher information for negative nonlinearity $\chi < 0$, the spin squeezing parameter does not monotonically decrease during generation by the quantum adiabatic brachistochrone. This is

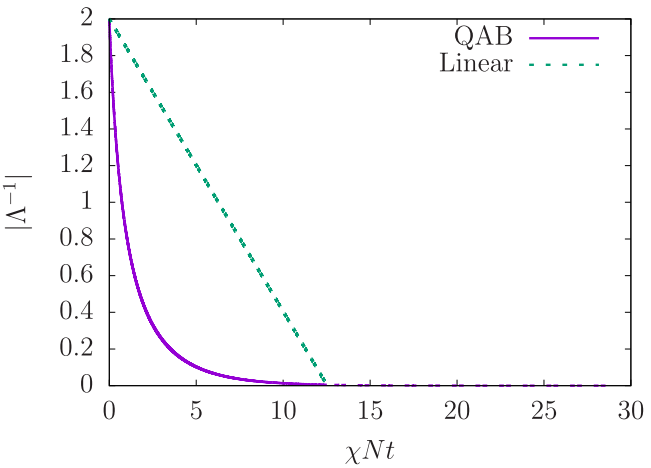

FIG. 8. An example of schedules of $|\Lambda^{-1}|$ with respect to the rescaled time χNt. The solid purple curve represents the schedule based on the quantum adiabatic brachistochrone during $|\Lambda^{-1}| : 2 \to 0.005$ and the dotted purple curve, which extends from the solid curve, is that during $|\Lambda^{-1}| : 0.005 \to 0$, for $C = -0.07$. The dotted green line is the corresponding linear schedule to the solid purple curve. Here $N = 100$.

because both (ΔJ_z) and $\langle J_x\rangle$ decrease and the spin squeezing parameter depends on the rate of these quantities.

We calculate the spin squeezed parameter with various values of the constant C and depict it in Fig. 10. As we can see, the quantum adiabatic brachistochrone decreases the spin squeezed parameter, i.e., increases the metrological usefulness, except for an ultrafast regime, $\chi N t_f \lesssim 3$. In this ultrafast regime, the spin squeezed parameter is not so small, and thus we are not as interested in this regime. Therefore, we can generally say that the quantum adiabatic brachistochrone improves the generation of a spin squeezed state. In contrast

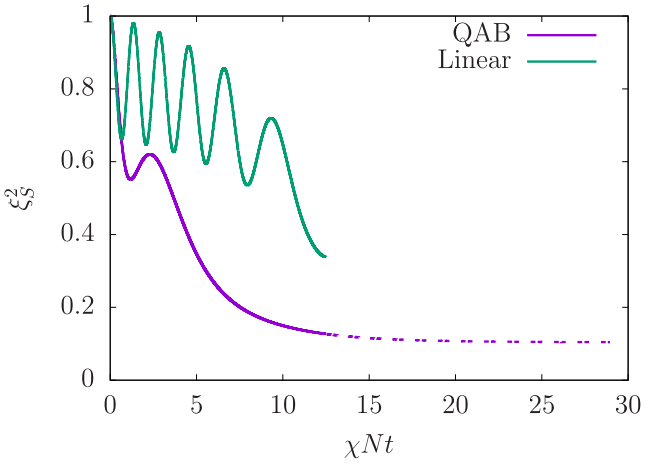

FIG. 9. Decrease in the spin squeezing parameter with respect to the rescaled time χNt. The solid purple curve represents the quantum adiabatic brachistochrone with $|\Lambda^{-1}| : 2 \to 0.005$ and the dotted purple curve extending from the solid curve is that with $|\Lambda^{-1}| : 0.005 \to 0$. The solid green curve represents the corresponding linear schedule with $|\Lambda^{-1}| : 2 \to 0.005$. Here $C = -0.07$ and $N = 100$.

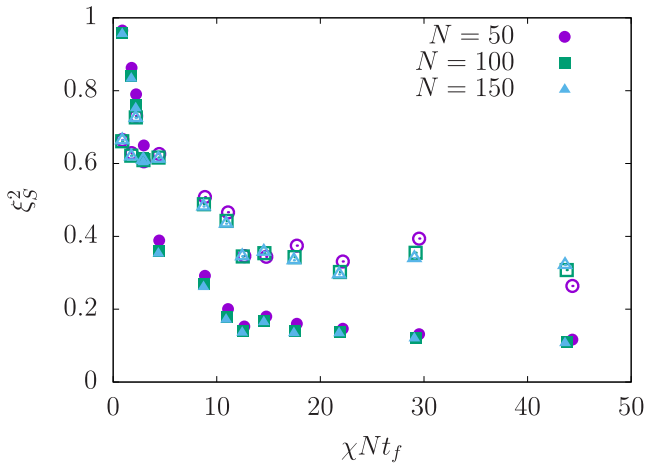

FIG. 10. The square of the spin squeezing parameter ξ_S^2 with respect to the rescaled generation time $\chi N t_f$. Filled symbols represent the quantum adiabatic brachistochrone and open symbols represent the linear schedule. Here $N = 50$ (purple circles), 100 (green squares), and 150 (cyan triangles).

to the case of negative nonlinearity $\chi < 0$, the system size dependence is quite small. For a small number of particles, $N = 50$, we calculate the square of the spin squeezing parameter over the long-time regime and plot it in Fig. 11. Notably, the spin squeezing parameter of a spin squeezed state generated via quantum adiabatic brachistochrone with $\chi N t_f \sim 20$ is approximately equal to that generated by the linear schedule with $\chi N t_f \sim 900$. This result shows the significance of using the quantum adiabatic brachistochrone for generation of a spin squeezed state.

We also calculate the improving rate of the spin squeezing parameter $R' = (\xi_S^{\mathrm{QAB}}/\xi_S^{\mathrm{Linear}})^2$ and plot it in Fig. 12. For a wide generation time region, a spin squeezed state generated via quantum adiabatic brachistochrone has more than double metrological usefulness compared with that generated by the linear schedule.

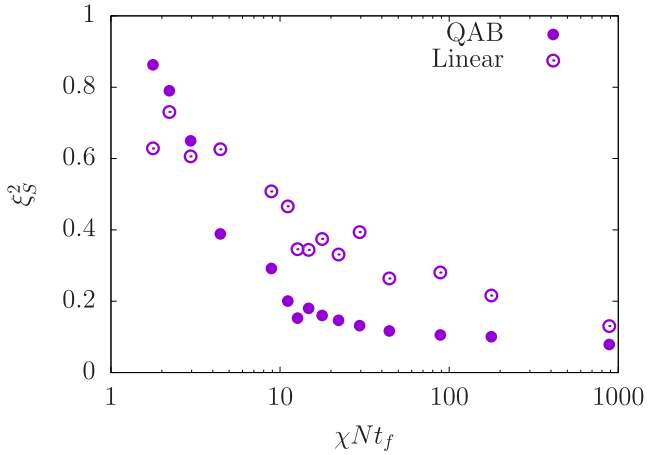

FIG. 11. Longer-time version of Fig. 10 for $N = 50$. Filled symbols represent the quantum adiabatic brachistochrone and open symbols represent the linear schedule.

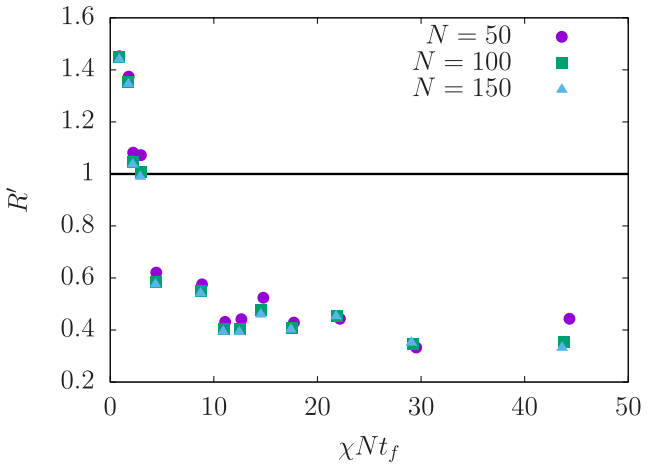

FIG. 12. The rate of improvement in the spin squeezing parameter $R' = (\xi_S^{\mathrm{QAB}}/\xi_S^{\mathrm{Linear}})^2$ with respect to the generation time $\chi N t_f$. Here $N = 50$ (purple circles), 100 (green squares), and 150 (cyan triangles).

Finally, we also calculate the quantum Fisher information of the generated spin squeezed states for comparison with the generated catlike states. It should be noted that the quantum Fisher information of a given state is larger than N, i.e., it is metrologically useful, if the spin squeezing parameter of the state is less than 1 because the inequality $F_Q \geqslant N/\xi_S^2$ holds [4]. Here we plot the quantum Fisher information scaled by N, F_Q/N, in Fig. 13. It clearly shows that the generated spin squeezed states are metrologically useful and the quantum adiabatic brachistochrone also improves the quantum Fisher information of spin squeezed states. However, it should be noted that the amount of quantum Fisher information of spin squeezed states is not as large compared with that of catlike states. Indeed, for a fixed scaled

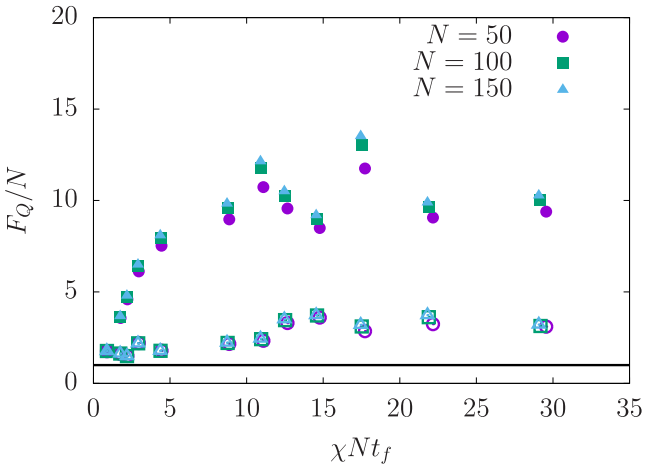

FIG. 13. The quantum Fisher information scaled by N, F_Q/N, with respect to the rescaled generation time $\chi N t_f$. Filled symbols represent the quantum adiabatic brachistochrone and open symbols represent the linear schedule. Here $N = 50$ (purple circles), 100 (green squares), and 150 (cyan triangles). Generated states are at least entangled and metrologically useful if F_Q/N surpasses the solid black line, $F_Q/N = 1$.

generation time $|\chi|Nt_f$, the quantum Fisher information of the generated spin squeezed states scales as $F_Q \propto N$ with $F_Q > N$, whereas that of the generated catlike states scales as $F_Q \propto N^2$. Moreover, the maximum amount of the quantum Fisher information of a spin squeezed state as the ground state of the bosonic Josephson junction Hamiltonian is $F_Q = N^2/2 + N$ [4], while that of a cat state is $F_Q = N^2$.

IV. SUMMARY

In this paper, we have considered the quantum adiabatic brachistochrone at a bosonic Josephson junction to find time-optimal schedules to create a catlike state and a spin squeezed state. In contrast to counterdiabatic driving at a bosonic Josephson junction, which requires a two-axis countertwisting interaction [36], the quantum adiabatic brachistochrone does not require any additional term. Moreover, we found that the optimized schedules are smooth and monotonically decreasing curves, which is rather realistic to implement in experiments compared with schedules designed by conventional optimal control theory [30,33,35]. Note that, for the creation of a catlike state, parity conservation plays an important role to avoid divergence of the quantum geometric tensor. It is also advantageous that generated states are automatically trapped by classical fixed points after generation. In the generation of both a catlike state and a spin squeezed state, we observed improvement of adiabaticity and an increase in metrological usefulness compared with the corresponding linear schedules.

Finally we discuss the possibility of realizing the present schemes in experiments. Our numerical simulation was studied by using the scaled time $|\chi|Nt$, and thus we first consider the accessible generation time from the viewpoint of nonlinearity. In Refs. [6] and [52], a Bose-Einstein condensate of ^{87}Rb shows $\chi = 2\pi \times 0.063$ Hz for $N = 200$–450 atoms. Therefore, the prefactor of the rescaled time can achieve $\chi N \approx 178\ \mathrm{s}^{-1}$. Similarly, in Ref. [10], it shows $\chi N \approx 188\ \mathrm{s}^{-1}$. For a time generating an intermediate-scale catlike state (about 80%–90% the size of the largest cat state) or a well-squeezed state ($\xi_S^2 \leqslant 0.2$), $|\chi|Nt_f \approx 10$; these values require a generation time $t_f \approx 50$ ms. Moreover, Ref. [7] shows $\chi = 0.49\ \mathrm{s}^{-1}$ with $N \approx 1250$ using the atom-chip-based technique and it achieves $\chi N \approx 613\ \mathrm{s}^{-1}$. For this parameter, the generation time is $t_f \approx 16$ ms. Note that a larger number of atoms leads to faster decay of entanglement. Therefore, one might be rather interested in generation with several hundred atoms. According to Ref. [10], the nonlinearity χ behaves as $\chi \propto 1/\sqrt{N}$, and thus it could be possible to achieve $\chi N \approx 368\ \mathrm{s}^{-1}$ for $N = 450$ using the atom-chip-based technique. It offers the generation time $t_f \approx 27$ ms. Entanglement generation experiments are typically performed over about 10–50 ms [5–13] and generated states are detectable even if about 10% of atoms are lost [49], and thus we expect that the generation time of the present scheme is realistic. Note that we have to simultaneously induce both nonlinearity and Rabi coupling as demonstrated in Ref. [52], and thus not all the above parameters are available. It should also be noted that negative nonlinearity is not directly realized in the above experimental setups. However, we can realize the present scheme with negative nonlinearity by considering the highest-energy eigenstate with positive nonlinearity as experimentally studied in Ref. [52] and as theoretically studied in Ref. [27] because the ground state with negative nonlinearity and the highest-energy eigenstate with positive nonlinearity are mathematically equivalent. This can be done by preparing the coherent spin state along the $(-x)$ axis instead of the x axis as the initial state. In summary, we believe that an intermediate-scale catlike state and a well-squeezed state will be generated using our scheme in the near-future.

[1] A. Acín, I. Bloch, H. Buhrman, T. Calarco, C. Eichler, J. Eisert, D. Esteve, N. Gisin, S. J. Glaser, F. Jelezko, S. Kuhr, M. Lewenstein, M. F. Riedel, P. O. Schmidt, R. Thew, A. Wallraff, I. Walmsley, and F. K. Wilhelm, The quantum technologies roadmap: A European community view, New J. Phys. **20**, 080201 (2018).

[2] V. Giovannetti, S. Lloyd, and L. Maccone, Advances in quantum metrology, Nat. Photon. **5**, 222 (2011).

[3] C. L. Degen, F. Reinhard, and P. Cappellaro, Quantum sensing, Rev. Mod. Phys. **89**, 035002 (2017).

[4] L. Pezzè, A. Smerzi, M. K. Oberthaler, R. Schmied, and P. Treutlein, Quantum metrology with nonclassical states of atomic ensembles, Rev. Mod. Phys. **90**, 035005 (2018).

[5] J. Estève, C. Gross, A. Weller, S. Giovanazzi, and M. K. Oberthaler, Squeezing and entanglement in a Bose-Einstein condensate, Nature **455**, 1216 (2008).

[6] C. Gross, T. Zibold, E. Nicklas, J. Estève, and M. K. Oberthaler, Nonlinear atom interferometer surpasses classical precision limit, Nature **464**, 1165 (2010).

[7] M. F. Riedel, P. Böhi, Y. Li, T. W. Hänsch, A. Sinatra, and P. Treutlein, Atom-chip-based generation of entanglement for quantum metrology, Nature **464**, 1170 (2010).

[8] K. Maussang, G. E. Marti, T. Schneider, P. Treutlein, Y. Li, A. Sinatra, R. Long, J. Estève, and J. Reichel, Enhanced and Reduced Atom Number Fluctuations in a BEC Splitter, Phys. Rev. Lett. **105**, 080403 (2010).

[9] C. F. Ockeloen, R. Schmied, M. F. Riedel, and P. Treutlein, Quantum Metrology with a Scanning Probe Atom Interferometer, Phys. Rev. Lett. **111**, 143001 (2013).

[10] H. Strobel, W. Muessel, D. Linnemann, T. Zibold, D. B. Hume, L. Pezzè, A. Smerzi, and M. K. Oberthaler, Fisher information and entanglement of non-Gaussian spin states, Science **345**, 424 (2014).

[11] W. Muessel, H. Strobel, D. Linnemann, D. B. Hume, and M. K. Oberthaler, Scalable Spin Squeezing for Quantum-Enhanced Magnetometry with Bose-Einstein Condensates, Phys. Rev. Lett. **113**, 103004 (2014).

[12] W. Muessel, H. Strobel, D. Linnemann, T. Zibold, B. Juliá-Díaz, and M. K. Oberthaler, Twist-and-turn spin squeezing in Bose-Einstein condensates, Phys. Rev. A **92**, 023603 (2015).

[13] R. Schmied, J.-D. Bancal, B. Allard, M. Fadel, V. Scarani, P. Treutlein, and N. Sangouard, Bell correlations in a Bose-Einstein condensate, Science **352**, 441 (2016).

[14] D. Leibfried, E. Knill, S. Seidelin, J. Britton, R. B. Blakestad, J. Chiaverini, D. B. Hume, W. M. Itano, J. D. Jost, C. Langer, R. Ozeri, R. Reichle, and D. J. Wineland, Creation of a six-atom 'Schrödinger cat' state, Nature **438**, 639 (2005).

[15] T. Monz, P. Schindler, J. T. Barreiro, M. Chwalla, D. Nigg, W. A. Coish, M. Harlander, W. Hänsel, M. Hennrich, and R. Blatt, 14-Qubit Entanglement: Creation and Coherence, Phys. Rev. Lett. **106**, 130506 (2011).

[16] A. Omran, H. Levine, A. Keesling, G. Semeghini, T. T. Wang, S. Ebadi, H. Bernien, A. S. Zibrov, H. Pichler, S. Choi, J. Cui, M. Rossignolo, P. Rembold, S. Montangero, T. Calarco, M. Endres, M. Greiner, V. Vuletić, and M. D. Lukin, Generation and manipulation of Schrödinger cat states in Rydberg atom arrays, Science **365**, 570 (2019).

[17] M. Kitagawa and M. Ueda, Squeezed spin states, Phys. Rev. A **47**, 5138 (1993).

[18] K. Mølmer and A. Sørensen, Multiparticle Entanglement of Hot Trapped Ions, Phys. Rev. Lett. **82**, 1835 (1999).

[19] A. Micheli, D. Jaksch, J. I. Cirac, and P. Zoller, Many-particle entanglement in two-component Bose-Einstein condensates, Phys. Rev. A **67**, 013607 (2003).

[20] L. D. Carr, D. R. Dounas-Frazer, and M. A. Garcia-March, Dynamical realization of macroscopic superposition states of cold bosons in a tilted double well, Europhys. Lett. **90**, 10005 (2010).

[21] M. A. García-March, D. R. Dounas-Frazer, and L. D. Carr, Macroscopic superposition of ultracold atoms with orbital degrees of freedom, Phys. Rev. A **83**, 043612 (2011).

[22] M. J. Steel and M. J. Collett, Quantum state of two trapped Bose-Einstein condensates with a Josephson coupling, Phys. Rev. A **57**, 2920 (1998).

[23] J. I. Cirac, M. Lewenstein, K. Mølmer, and P. Zoller, Quantum superposition states of Bose-Einstein condensates, Phys. Rev. A **57**, 1208 (1998).

[24] A. J. Leggett and F. Sols, Comment on "Phase and Phase Diffusion of a Split Bose-Einstein Condensate,"Phys. Rev. Lett. **81**, 1344 (1998).

[25] J. Javanainen and M. Y. Ivanov, Splitting a trap containing a Bose-Einstein condensate: Atom number fluctuations, Phys. Rev. A **60**, 2351 (1999).

[26] C. Lee, Adiabatic Mach-Zehnder Interferometry on a Quantized Bose-Josephson Junction, Phys. Rev. Lett. **97**, 150402 (2006).

[27] E. Yukawa, G. J. Milburn, and K. Nemoto, Fast macroscopic-superposition-state generation by coherent driving, Phys. Rev. A **97**, 013820 (2018).

[28] D. Spehner, K. Pawlowski, G. Ferrini, and A. Minguzzi, Effect of one-, two-, and three-body atom loss processes on superpositions of phase states in Bose-Josephson junctions, Eur. Phys. J. B **87**, 157 (2014).

[29] K. Pawłowski, M. Fadel, P. Treutlein, Y. Castin, and A. Sinatra, Mesoscopic quantum superpositions in bimodal Bose-Einstein condensates: Decoherence and strategies to counteract it, Phys. Rev. A **95**, 063609 (2017).

[30] J. Grond, J. Schmiedmayer, and U. Hohenester, Optimizing number squeezing when splitting a mesoscopic condensate, Phys. Rev. A **79**, 021603(R) (2009).

[31] B. Juliá-Díaz, E. Torrontegui, J. Martorell, J. G. Muga, and A. Polls, Fast generation of spin-squeezed states in bosonic Josephson junctions, Phys. Rev. A **86**, 063623 (2012).

[32] A. Yuste, B. Juliá-Díaz, E. Torrontegui, J. Martorell, J. G. Muga, and A. Polls, Shortcut to adiabaticity in internal bosonic Josephson junctions, Phys. Rev. A **88**, 043647 (2013).

[33] T. Pichler, T. Caneva, S. Montangero, M. D. Lukin, and T. Calarco, Noise-resistant optimal spin squeezing via quantum control, Phys. Rev. A **93**, 013851 (2016).

[34] D. Stefanatos and E. Paspalakis, Maximizing entanglement in bosonic Josephson junctions using shortcuts to adiabaticity and optimal control, New J. Phys. **20**, 055009 (2018).

[35] M. Lapert, G. Ferrini, and D. Sugny, Optimal control of quantum superpositions in a bosonic Josephson junction, Phys. Rev. A **85**, 023611 (2012).

[36] T. Hatomura, Shortcuts to adiabatic cat-state generation in bosonic Josephson junctions, New J. Phys. **20**, 015010 (2018).

[37] Y. C. Liu, Z. F. Xu, G. R. Jin, and L. You, Spin Squeezing: Transforming One-Axis Twisting into Two-Axis Twisting, Phys. Rev. Lett. **107**, 013601 (2011).

[38] C. Shen and L.-M. Duan, Efficient spin squeezing with optimized pulse sequences, Phys. Rev. A **87**, 051801(R) (2013).

[39] J.-Y. Zhang, X.-F. Zhou, G.-C. Guo, and Z.-W. Zhou, Dynamical spin squeezing via a higher-order Trotter-Suzuki approximation, Phys. Rev. A **90**, 013604 (2014).

[40] T. Opatrný, M. Kolář, and K. K. Das, Spin squeezing by tensor twisting and Lipkin-Meshkov-Glick dynamics in a toroidal Bose-Einstein condensate with spatially modulated nonlinearity, Phys. Rev. A **91**, 053612 (2015).

[41] D. Kajtoch and E. Witkowska, Spin squeezing in dipolar spinor condensates, Phys. Rev. A **93**, 023627 (2016).

[42] A. del Campo, M. M. Rams, and W. H. Zurek, Assisted Finite-Rate Adiabatic Passage Across a Quantum Critical Point: Exact Solution for the Quantum Ising Model, Phys. Rev. Lett. **109**, 115703 (2012).

[43] A. T. Rezakhani, W.-J. Kuo, A. Hamma, D. A. Lidar, and P. Zanardi, Quantum Adiabatic Brachistochrone, Phys. Rev. Lett. **103**, 080502 (2009).

[44] A. T. Rezakhani, D. F. Abasto, D. A. Lidar, and P. Zanardi, Intrinsic geometry of quantum adiabatic evolution and quantum phase transitions, Phys. Rev. A **82**, 012321 (2010).

[45] M. Demirplak and S. A. Rice, Adiabatic population transfer with control fields, J. Phys. Chem. A **107**, 9937 (2003).

[46] M. V. Berry, Transitionless quantum driving, J. Phys. A: Math. Theor. **42**, 365303 (2009).

[47] D. Guéry-Odelin, A. Ruschhaupt, A. Kiely, E. Torrontegui, S. Martínez-Garaot, and J. G. Muga, Shortcuts to adiabaticity: Concepts, methods, and applications, arXiv:1904.08448 .

[48] R. Gati and M. K. Oberthaler, A bosonic Josephson junction, J. Phys. B: At. Mol. Opt. Phys. **40**, R61 (2007).

[49] T. Hatomura and K. Pawłowski, Superadiabatic generation of cat states in bosonic Josephson junctions under particle losses, Phys. Rev. A **99**, 043621 (2019).

[50] J. E. Avron, R. Seiler, and L. G. Yaffe, Adiabatic theorems and applications to the quantum Hall effect, Commun. Math. Phys. **110**, 33 (1987).

[51] K. Takahashi, Transitionless quantum driving for spin systems, Phys. Rev. E **87**, 062117 (2013).

[52] T. Zibold, E. Nicklas, C. Gross, and M. K. Oberthaler, Classical Bifurcation at the Transition from Rabi to Josephson Dynamics, Phys. Rev. Lett. **105**, 204101 (2010).